

# Simulation of the formation of two-dimensional Coulomb liquids and solids in dusty plasmas

Helen H. Hwang<sup>a)</sup> and Mark J. Kushner<sup>b)</sup>

Department of Electrical and Computer Engineering, University of Illinois, 1406 West Green Street, Urbana, Illinois 61801

(Received 6 January 1997; accepted for publication 4 June 1997)

Dust particle transport in low-temperature plasmas has recently received considerable attention due to the desire to minimize contamination of wafers during plasma processing of microelectronics devices. Laser light scattering observations of dust particles near wafers in reactive-ion-etching (RIE) radio frequency (rf) discharges have revealed clouds which display collective behavior. These observations have motivated experimental studies of the Coulomb liquid and solid properties of these systems. In this paper, we present results from a two-dimensional model for dust particle transport in RIE rf discharges in which we include particle-particle Coulomb interactions. We predict the formation of Coulomb liquids and solids. These predictions are based both on values of  $\Gamma > 2$  (liquid) and  $\Gamma > 170$  (solid), where  $\Gamma$  is the ratio of electrostatic potential energy to thermal energy, and on crystal-like structure in the pair correlation function. We find that Coulomb liquids and solids composed of trapped dust particles in RIE discharges are preferentially formed with increasing gas pressure, decreasing particle size, and decreasing rf power. We also observe the ejection of particles from dust crystals which completely fill trapping sites, as well as lattice disordering followed by annealing and refreezing. © 1997 American Institute of Physics. [S0021-8979(97)06117-3]

## I. INTRODUCTION

Dust particle transport in partially ionized plasmas has been the focus of many recent investigations as a consequence of concern over particle contamination of wafers during plasma processing of microelectronics devices.<sup>1</sup> Particles (10 s nm to a few microns in size) resemble floating bodies in plasmas and negatively charge to balance the flux of electrons and ions to the their surfaces. As a consequence, the transport of these particles is governed by both mechanical (fluid drag, thermophoresis, gravity) and electrical (ion drag, electrostatic) forces. Observations of particles accumulating in thin layers near the edge of sheaths in reactive ion etching (RIE) radio frequency (rf) discharges have been explained by there being a balance between ion drag forces (accelerating particles out of the plasma), electrostatic forces (accelerating particles towards the peak in the plasma potential, usually in the center of the plasma) and, in the case of large particles (many to 10s  $\mu\text{m}$ ), gravity. In many cases, particularly when the particle densities are large, the particles accumulate in clouds which display nearly rigid body character when perturbed.<sup>2</sup> This behavior has been attributed to interparticle Coulomb forces which produce collective motion, a system typically referred to as a Coulomb liquid or solid.

The Coulomb coupling parameter which characterizes a Coulomb liquid or solid is

$$\Gamma = \frac{\left( \frac{Q^2}{4\pi\epsilon_0 d} \right)}{k_B T} \quad (1)$$

where  $k_B$  is the Boltzmann's constant, and particles have charge  $Q$ , average interparticle spacing  $d$ , and kinetic temperature  $T$ .  $\Gamma$  is a measure of the potential energy of particles due to Coulomb interactions compared to their thermal energy. Ichimaru suggests that three-dimensional Coulomb fluids are obtained for  $\Gamma > 2$ ,<sup>3</sup> while Slatery *et al.* propose that the particles form a Coulomb solid for  $\Gamma > 170$ .<sup>4</sup> These cut-offs are likely to be lower for two-dimensional structures.<sup>3</sup> These critical values for  $\Gamma$  are only strictly correct for one-component plasmas and so should be considered approximate guides for the discussion that follows.

The propensity for dust particles to form Coulomb liquid or solids in plasma processing discharges was first proposed by Ikezi<sup>5</sup> for conditions where the electrostatic forces between the particles dominate over their thermal kinetic energy. Subsequently, observations of Coulomb liquid and solids of dust particles have been made in a variety of laboratory discharges.<sup>6-10</sup> Perhaps the most common Coulomb fluid obtained in plasma processing discharges is during the plasma deposition of silicon films using silane gas mixtures. In these discharges, particle densities can be sufficiently large so that the majority of the negative charge in the plasma resides on particles (as opposed to electrons). For example, Boufendi *et al.*<sup>6</sup> observed 100 nm diameter particles in an Ar/SiH<sub>4</sub>=96/4 rf parallel plate discharge at 120 mTorr. They measured particle densities exceeding  $10^8 \text{ cm}^{-3}$ , and estimated that the particle charge was  $Q/q \approx 50$ , resulting in  $\Gamma \approx 50$ .

Crystalline structures or lattices of dusty particles were first quantitatively observed by laser light scattering by Chu *et al.*<sup>7</sup> SiO<sub>2</sub> particles 10  $\mu\text{m}$  in diameter were generated in an Ar/SiH<sub>4</sub>/O<sub>2</sub> rf discharge. Two-dimensional structures were observed at low particle density and three-dimensional structures were found at high particle densities. They found that

<sup>a)</sup>Present address: NASA Ames Research Center, MS 230-3, Moffett Field, CA 94035. Electronic mail: hwang@dml.arc.nasa.gov

<sup>b)</sup>Author to whom correspondence should be addressed. Electronic mail: mjk@uiuc.edu

particles froze into a Coulomb solid only at moderately high buffer gas pressures ( $>100$ s mTorr) which provided sufficient viscous fluid drag to cool the particles, thereby increasing  $\Gamma$ . Due to the polydisperse size distribution of their particles, the solids Chu *et al.* observed had varying interparticle distance and lacked significant long range order.

Coulomb solids forming highly ordered lattices were observed by Thomas *et al.*<sup>8</sup> A rf discharge sustained in 1.5 Torr Ar was seeded with  $7.0 \pm 0.2 \mu\text{m}$  diameter particles. By laser light scattering, a Coulomb solid consisting of 18 planar layers was observed near the plasma sheath boundary. Hexagonal lattices having particle densities of  $>4 \times 10^4 \text{ cm}^{-3}$ , interparticle spacings of  $250 \mu\text{m}$  and kinetic temperatures of 310 K were measured, producing  $\Gamma > 20\,000$ . They observed that at higher rf discharge powers, the particles moved “violently” and did not have equilibrium positions in the crystals. That is, they appeared more liquidlike. Similar hexagonal lattices were observed by Trottenberg *et al.* for monodisperse particles ( $9.4 \mu\text{m}$  diameter) particles in argon rf parallel plate discharges.<sup>9</sup> They found that the interparticle spacing decreased with increasing power deposition. For discharges of 30 W at 560 mTorr gas pressure, crystals having  $\Gamma \approx 1550$  were obtained.

Pieper *et al.*<sup>10</sup> observed stable three-dimensional Coulomb solids having body-centered-cubic and hexagonal lattices for monodisperse  $9.4 \mu\text{m}$  diameter particles in rf discharges sustained in He, Ar, Kr, and Xe. For plasma densities of  $\approx 6 \times 10^8 \text{ cm}^{-3}$  in Kr at 1.3 Torr, hexagonal lattices having interparticle spacing of  $128 \mu\text{m}$  were observed. It was generally observed that higher pressures produced more stable lattices, presumably due to more rapid cooling of the particles. They observed that adding particles to stable lattices generally increased the number of layers of particles, however particles eventually escaped from the edge of the particle cloud lattice until the original number of layers was restored.

Farouki and Hamaguchi<sup>11</sup> computationally studied phase transitions of dust particles in plasmas by performing a Monte Carlo simulation for particles interacting through a screened Coulomb potential. By “seeding” a computational volume with particles having a predetermined value of average  $\Gamma$ , they classified the resulting arrangement of particles as either fluid or solid. They observed that phase transitions between fluids and solids occurred for  $\Gamma = 30\text{--}100$ , a value which depended on the number of particles in their system.

From these studies, the following scaling laws for dust particles forming Coulomb solids in rf discharges can be formulated: Interparticle distance in the lattice decreases with increasing discharge power;<sup>8–10</sup> interparticle distance is dependent on particle size;<sup>7</sup> the lattice is less stable with large particles;<sup>7,10</sup> particles in a Coulomb solid can escape from the lattice, forming a dislocation, and the lattice subsequently anneals.<sup>10</sup>

In this paper we discuss results from a two-dimensional computer model for the formation of Coulomb liquids and solids in rf parallel plate discharges sustained in argon with the goal of investigating these scaling laws. This model is an extension of a previously described simulation for dust particle transport in plasmas called the dust transport simulation

(DTS).<sup>12,13</sup> We find that the formation of Coulomb liquids and solids, as characterized by  $\Gamma$ , depends critically on rf power and particle size. Lattices are both less stable and take longer to form as the particle size and rf power increase. We also observe the ejection of particles from lattices which fully fill a trapping site. Energetic particles incident onto otherwise stable lattices may “melt” the solid by converting their kinetic energy into thermal energy. The model we used in this investigation is described in Sec. II. Results from our study of Coulomb liquids and solids are in Sec. III, followed by our concluding remarks in Sec. IV.

## II. DESCRIPTION OF THE MODEL

Our model for strongly coupled dust particle transport is based on the previously described DTS.<sup>12,13</sup> The model is a two-dimensional ( $r, z$ ) Monte Carlo simulation in which the trajectories of dust particles are integrated based on mechanical and electrical forces. The forces included in the model are ion drag, fluid drag, electrostatic, thermophoretic, self-diffusive, and gravitational forces, along with Brownian motion. In this model, we do not take into account the perturbation of plasma properties by the dust particles. Previous works by others have addressed this issue and found that, for example, the negatively charged dust particles focus ions flowing into the crystal.<sup>14</sup> The equilibrium configuration of the crystal can be influenced by this asymmetric ion flow. In this work, we assume that the charge on the particle is in quasiequilibrium with the local plasma conditions. In doing so, the charge on the particle is given by<sup>15,16</sup>

$$Q = C\varphi_0, \quad C = 4\pi\epsilon_0 a(1 + a/\lambda_L), \quad (2)$$

where  $C$  is the capacitance of the dust particle,  $\lambda_L$  is the linearized Debye length,  $a$  is the particle radius, and  $\varphi_0$  is the particle potential. The linearized Debye length (for electrons and one positive ion species) is<sup>15</sup>

$$\frac{1}{\lambda_L} = \left[ \frac{n_e q^2}{\epsilon_0} \left( \frac{1}{kT_e} + \frac{1}{2E_I} \right) \right]^{1/2} \quad (3)$$

where  $T_e$  is the electron temperature,  $n_e$  is the electron density, and  $E_I$  is the ion energy. The particle electrical floating potential is obtained by requiring that the negative and positive currents to the particle are equal. Assuming orbital-motion-limited trajectories (and assuming here that there is one positive ion species and electrons), the particle currents are

$$j_e = \left( \frac{3kT_e}{\pi m_e} \right)^{1/2} \exp\left( \frac{q\varphi_0}{kT_e} \right), \quad j_I = \left( \frac{2E_I}{M_I} \right)^{1/2} \left( 1 - \frac{q\varphi_0}{E_I} \right). \quad (4)$$

The ion drag cross section we used is that derived by Kilgore *et al.*<sup>15</sup>

$$\sigma = b^2 c_1 \ln \left[ 1 + \frac{c_2}{(b/\lambda_L)^2} \right], \quad b = \frac{Q^2}{4\pi\epsilon_0 E_I}, \quad (5)$$

where  $c_1 = 0.9369$  and  $c_2 = 61.32$  are semiempirical values. This expression yields essentially the same cross section as that obtained from molecular dynamics simulations of the ion-dust particle interaction.<sup>17</sup>

In addition to these mechanical and electrical forces, we also included particle-particle forces resulting from Coulomb interactions between particles. The screened electrical potential distance  $r$  from a particle is

$$\varphi(r) = \varphi_0 \cdot \frac{a}{r} \cdot \exp\left(-\frac{(R-a)}{\lambda_L}\right). \quad (6)$$

Accounting for the plasma screening, the interparticle Coulomb force between particles separated by  $R$  is approximated by

$$\vec{F} = \frac{Q_1 Q_2}{4\pi\epsilon_0} \cdot \frac{1}{R} \cdot \left(\frac{1}{R} + \frac{1}{\lambda_L}\right) \cdot \exp\left(-\frac{(R-a)}{\lambda_L}\right) \frac{\vec{R}}{R}. \quad (7)$$

Directly including particle-particle interactions into the acceleration terms in a Monte Carlo simulation implies an  $N^2$  scaling for computer time (where  $N$  is the number of pseudoparticles). Typically 5000–10 000 pseudoparticles are used in the simulation. To reduce the scope of the calculation, we restricted Coulomb interactions to only particles residing within a specified interaction distance of each other. This distance was determined by parameterizing the model. For computational purposes, we found it convenient to bin particles by the mesh cell they occupied. On a mesh with spacing 0.2 cm, interacting particles in adjacent cells or cells within  $5\lambda_L$  was sufficient. We note that Farouki and Hamaguchi<sup>11</sup> did not use a maximum interaction distance in their studies and found that the value of  $\Gamma$  at which phase transitions occurred depended on the size of the system. Although we did not observe this trend, the boundary conditions in our system are sufficiently different compared to Farouki and Hamaguchi so that the different observations may not be particularly relevant.

Plasma properties (electron and ion densities, ion neutral fluxes, electrostatic potential, and electric fields) required as input to the DTS are obtained from the Hybrid Plasma Equipment Model (HPEM). The HPEM is a comprehensive simulator of low pressure plasma reactors, and has been described in detail in Refs. 18–20. For the results discussed here, the following options in the HPEM were used. The electron transport coefficients were obtained using the electron energy equation module. Continuity and momentum equations were solved for ions and neutral particles, while only the continuity equation was solved for electrons. Poisson's equation was solved using a semiexplicit technique.

To quantify the character of the Coulomb liquid or solid dust particle clouds in our plasmas, we utilized two metrics; the Coulomb coupling parameter  $\Gamma$ , and the pair correlation function (PCF),  $g(r)$ . To account for the screened charge on the dust particles, the Coulomb coupling parameter for a collection of  $N$  particles is

$$\Gamma = \frac{1}{N} \sum_{i=1}^N \Gamma_i, \quad \Gamma_i = \frac{\frac{Q_i}{4\pi\epsilon_0} \cdot \sum_j \frac{Q_j}{R_{ij}} \cdot \exp\left(-\frac{R_{ij}-a}{\lambda_L}\right)}{\frac{1}{2} m v_i^2}, \quad (8)$$

where  $v_i$  is the rms speed of the particle. The particle parameter, as defined in Eq. (1), is a function of the particle's temperature whereas we have used the particles kinetic en-

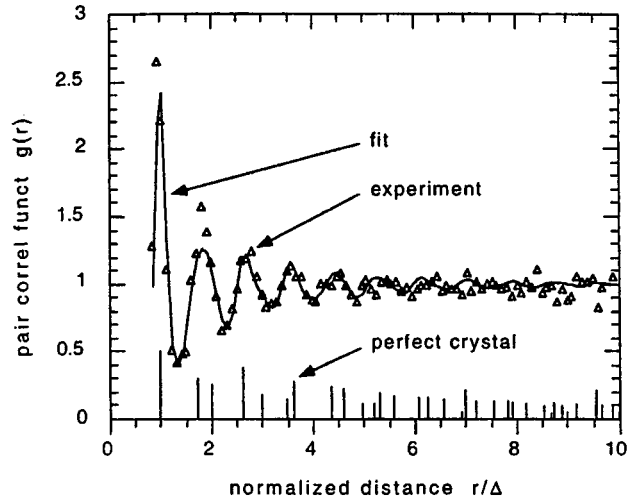


FIG. 1. Typical pair correlation function (PCF) for experimentally measured particle positions (Ref. 8) as fit by Quinn *et al.* (Ref. 22). The interparticle spacing is  $290 \mu\text{m}$  for  $3.5 \mu\text{m}$  particles in an argon rf discharge at 0.4 W and 1.5 Torr.

ergy as a scaling factor. The particle temperature in RIE discharges is, at least prior to solidification of the crystal, poorly defined since the particles kinetic energy is dominated by drift motion. The effective temperature of a particle can, however, be defined analogously to ions in swarm experiments, as  $3/2kT_{\text{eff}} = 3/2kT_{\text{thermal}} + 1/2m v_{\text{drift}}^2$ .<sup>21</sup> For example, a  $0.5 \mu\text{m}$  particle with a directed velocity of 10 cm/s corresponds to  $3 \times 10^4$  K of effective temperature. Neglecting fluid-drag effects which cool the particles, particles ultimately convert their directed energy obtained from ion drag and electrostatic acceleration into randomized thermal energy through Coulomb collisions with other particles. We will see that particles having large drift velocities, and hence large  $T_{\text{eff}}$ , and which impact on a Coulomb solid having low  $\Gamma$ , convert their directed energy into thermal energy. The thermal energy is conducted through the crystal, resulting in local melting.

To examine the phases of the structures that form (solid versus liquid), the pair correlation function (PCF),  $g(r)$ , is calculated. The PCF is the probability of finding two particles separated by a distance  $r$ , as compared to that for an unstructured random distribution of particles. The PCF is calculated using the method described by Quinn *et al.*<sup>22</sup> A particle is chosen as the center point or test particle. The remaining particles in a specified region are then ‘‘binned’’ according to their distance to the test particle. These particle counts are then divided by the annular area defined by their distance from the test particle, and are normalized by the resulting average particle density. This procedure is repeated using all particles in the region as the test particle and the results averaged. In an infinite crystal,  $g(r)$  would asymptotically approach unity at large  $r$ . Peaks in  $g(r)$  at small  $r$  correspond to first, second, and next nearest neighbors. For example, a typical experimental PCF derived from the data of Thomas *et al.*<sup>8</sup> and Quinn *et al.*<sup>22</sup> is shown in Fig. 1 for a lattice in an Ar, 0.4 W, 1.5 Torr rf discharge. The  $3.5 \mu\text{m}$  particles form a Coulomb solid with interparticle spacing of

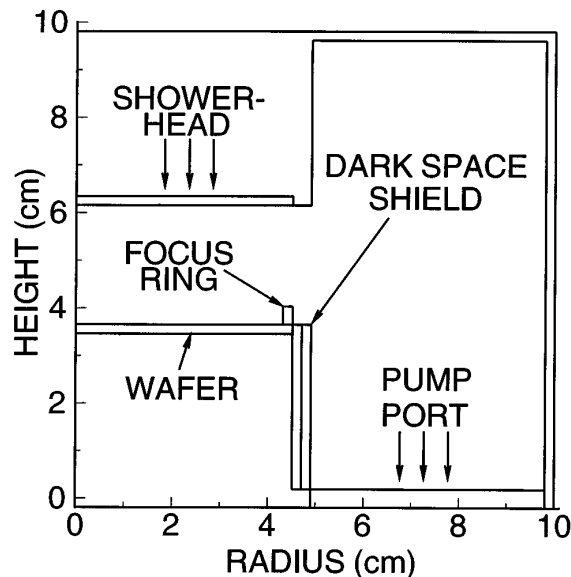


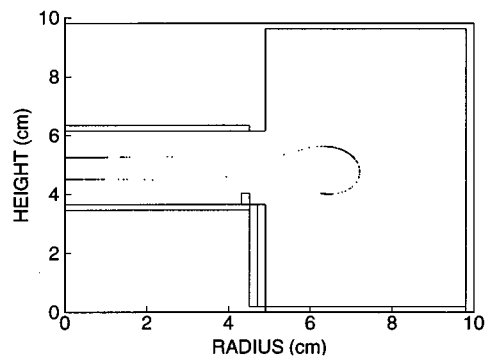
FIG. 2. Schematic of the modified GEC reference cell used in the simulations. Ar flows from a showerhead in the upper electrode (grounded) and out through the pump port. The lower electrode is powered. The focus ring was added to the standard GEC reference cell to aid in confinement of particles.

250  $\mu\text{m}$ , and  $\Gamma$  is estimated to be  $>20\,700$ . Although the PCF does not have a perfect crystal signature, it does have nine well-defined peaks and has the characteristic shape of a Coulomb solid. The PCF approaches unity at large distances, as this particular crystal is over 20 layers thick.

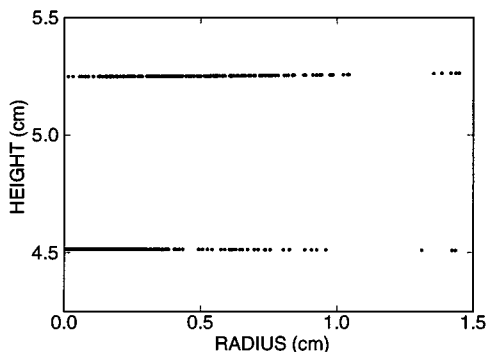
### III. CHARACTERISTICS OF COULOMB FLUIDS AND SOLIDS IN RIE DISCHARGES

The reactor geometry used for this study is shown in Fig. 2. The rf discharge is a modified GEC reference cell, with a showerhead in the grounded upper electrode and a dielectric focus ring on the lower electrode which is powered at 13.56 MHz. The focus ring was employed to help confine particles. The gas is argon at 100 mTorr with a flow rate of 30 sccm which is exhausted through the pump port surrounding the lower electrode. For a power deposition of 7.3 W, the average electron temperature between the electrodes is  $\sim 4.3$  eV and the peak electron density is  $2 \times 10^9 \text{ cm}^{-3}$ . Dust particles are initially generated randomly between the electrodes with radii between 0.25 and 1.0  $\mu\text{m}$ , and have a mass density of  $2.33 \text{ g cm}^{-3}$ , akin to that of amorphous silicon. The simulation time, unless specified otherwise, is 0.3 s after release of the particles. We purposely chose particles sizes which are small enough so that gravity is not an important factor in determining the configuration of the crystal.

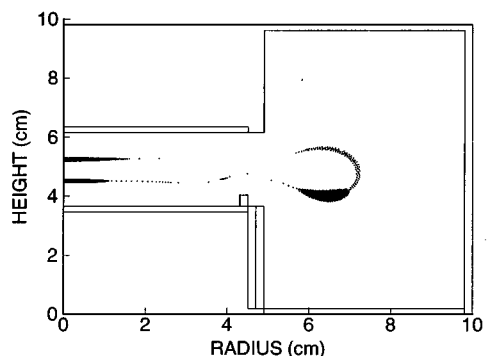
The gross effects of including Coulomb interactions between 0.5  $\mu\text{m}$  particles are shown in Fig. 3 where particle trapping locations are shown with and without these forces in the model. In the absence of Coulomb interactions, the particles are trapped in a single layer adjacent to the powered and grounded electrode sheaths. This trapping results from a balance between the electrostatic and ion drag forces. There is also a trapping site in the periphery of the reactor. Gas flow has “blown” particles to the virtual sheath where the



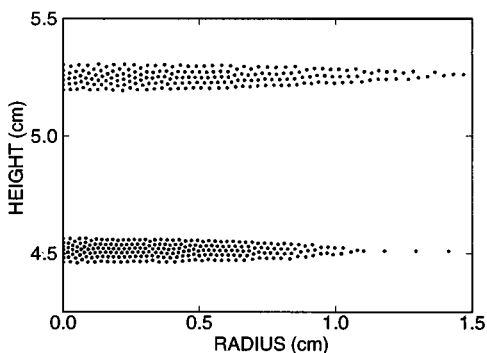
(a)



(b)



(c)



(d)

FIG. 3. Particle positions (0.5  $\mu\text{m}$ ) in an Ar discharge (100 mTorr, 7.3 W) after 0.3 s. (a) Particle locations obtained while excluding Coulomb interactions. (b) Expanded view of particle positions without Coulomb interactions. (c) Particle locations obtained while including Coulomb interactions. (d) Expanded view of particle positions with Coulomb interactions. Including Coulomb interactions produces clouds of finite thickness which have large  $\Gamma$  and long range structure, in this case a hexagonal lattice.

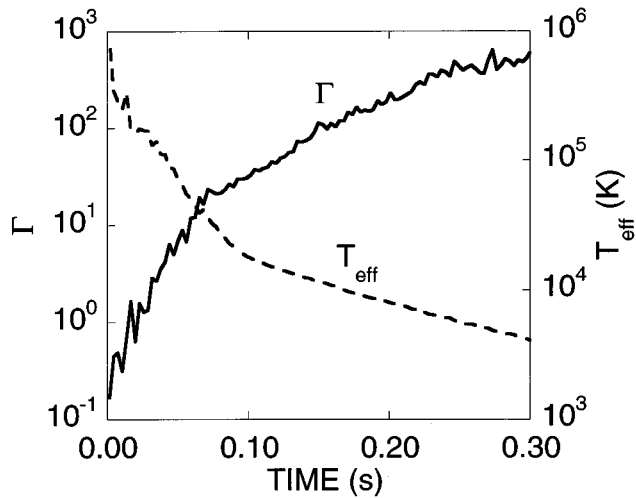


FIG. 4. Evolution of  $\Gamma$  and effective temperature for particles in the lower lattice of Fig. 3 [100 mTorr, Ar discharge (5.5 W)]. The average particle temperature decreases due to loss of energetic particles to surfaces and fluid drag cooling. Particle cooling results in increasing  $\Gamma$  and eventual Coulomb solidification.

plasma density decays to low values (although this is not at the surface of a material). Here, the trapping results from a balance between gas flow and electrostatic forces.

When including Coulomb interactions, the particles form multilayer “clouds” of finite thickness, both at the trapping locations between the electrodes and in the outer trapping regions. Closeup views of the trapping locations between the electrodes ( $0 < r < 1.5$  cm,  $4.25 < z < 5.5$  cm) show these clouds to be hexagonal lattices having 5–7 layers. The particle spacing is smaller in the lower lattice compared to the upper lattice. This results from a higher plasma density near the powered electrode, producing a smaller  $\lambda_L$ , and thus smaller shielding distances between the particles. Formation of these lattices requires both cohesive and repulsive forces. The repulsive forces, in this case Coulomb interactions, provide the means whereby particles arrange themselves in a minimum potential energy configuration. There must, however, also be a cohesive force which prevents particles at the periphery of the lattice from “melting away” since they are not confined by a symmetric array of Coulomb forces. In these examples, the cohesive forces are the electrostatic and ion drag forces, which, in the absence of Coulomb interactions, would produce planar trapping of the particles. In fact, the smaller lattice spacing near the lower electrode results, in part, from larger ion drag and electrostatic forces providing larger cohesive forces. We note that Melzer *et al.*<sup>23</sup> have measured particle temperatures of many 1000s K, albeit for larger ( $9.4 \mu\text{m}$ ) particles, in crystals formed in rf discharges at pressures of 100s mTorr.

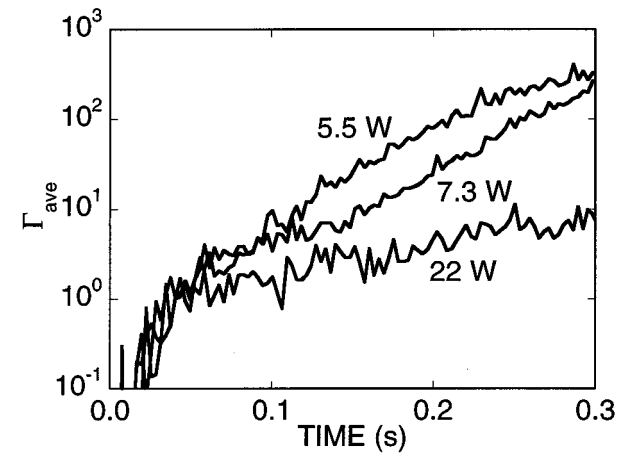
To confirm that the particles do assemble into a Coulomb liquid or solid, the Coulomb coupling parameter  $\Gamma$  and effective temperature of the particles in the lower trapping cloud are plotted as a function of time after releasing the particles in Fig. 4 for a 5.5 W discharge. When the particles are initially released in the plasma, they are rapidly accelerated by ion drag forces, producing a large  $T_{\text{eff}}$ . Since at this

time the particles also have large spacing, the resulting  $\Gamma$  is small. As time progresses, highly energetic particles leave the plasma which contributes to lowering  $T_{\text{eff}}$ , an effect akin to diffusion cooling of electrons. As particles trap at the sheath edge, they continue to cool as a result of fluid drag. The progressive lowering of  $T_{\text{eff}}$  due to fluid drag cooling of the particles is largely responsible for the increase in  $\Gamma$  to values resembling Coulomb fluids and eventually solids.  $T_{\text{eff}}$  is still significantly above the gas temperature of 300 K after 0.3 s due to particles slowly joining the crystal at large radius. When these particles collide with the crystal, their large translation energy is dissipated into thermal energy, which is then distributed through the crystal by elastic collisions between the particles. We have found that many to tens of seconds are required for the Coulomb solid to fully form and reach a full equilibrium, similar to experimental observations.

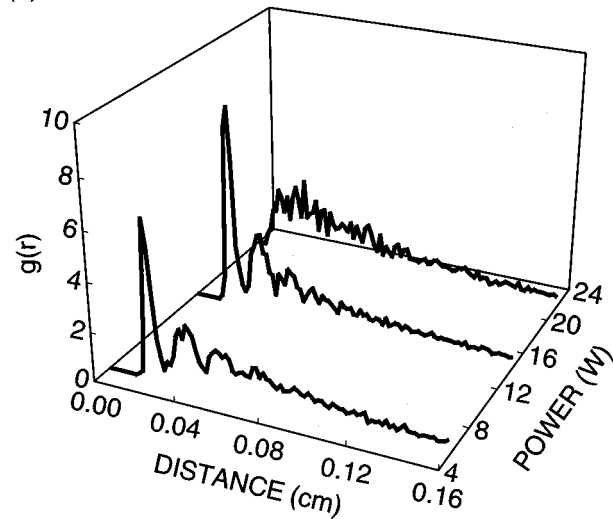
Experimental observations have also shown that higher discharge powers produce less stable lattices. We investigated this scaling by varying the rf power in the model. The resulting  $\Gamma$  as a function of time, PCF, and interparticle spacing are shown in Fig. 5 for particles in the lower lattice. The interparticle spacing and PCF are shown for 0.3 s after release of the particles. The reactor power affects the lattice structure by, in part, determining the magnitude of the ion fluxes that generate the ion-drag force. At low power (5.5 W), the smaller ion fluxes produce smaller ion-drag forces which, in turn, result in smaller kinetic energies (and temperatures) of the particles. Smaller particle temperatures enable higher values of  $\Gamma$ , as shown in Fig. 5(a).  $\Gamma$  increases with time and exceeds 100 by 0.14 s, producing a Coulomb solid. As the power is increased (from 5.5 to 22 W),  $\Gamma$  increases more slowly with time as the particles require more time to thermalize. At best, the particles form Coulomb liquids at the higher power, rather than solids, due to the larger particle temperatures produced by ion drag. The high dust velocities and the inertia of the particles (and their subsequently higher temperatures) make it difficult for a stable lattice to form.

The PCFs for 5.5, 14.3, and 22 W cases after 0.3 s are shown in Fig. 5(b). At the lower powers,  $g(r)$  resembles that of a solid, similar to the experimentally derived PCF shown in Fig. 1. At least four distinct peaks can be distinguished in the PCF at 5.5 and 14.3 W. This is a signature of a solid with long range order. The lower particle temperatures resulting from the smaller ion drag forces experienced at low power ultimately allow particles to cool sufficiently through fluid drag to form Coulomb solids. At higher powers the PCF has one broad peak corresponding to nearest neighbors, but lacks secondary peaks. At best, this PCF resembles that of a liquid. A phase transition between a Coulomb solid and Coulomb liquid takes place between powers of 15 and 20 W. The solid-to-liquid transition when increasing rf power has been experimentally observed by Melzer *et al.*, an effect they attribute to an increasing particle temperature.<sup>23</sup>

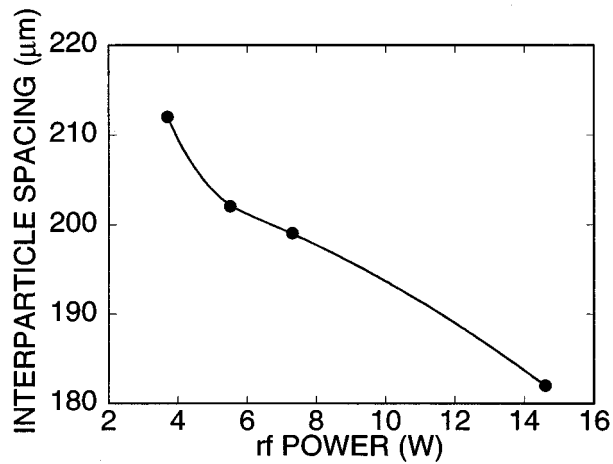
The interparticle distance,  $d$ , as a function of rf power is shown in Fig. 5(c). This distance is the first nearest neighbor spacing obtained from the PCFs. Typical interparticle spacings are 150–250  $\mu\text{m}$ . Although lattices are more difficult to



(a)



(b)



(c)

FIG. 5. Particle parameters while varying rf discharge power. (a) Coulomb coupling parameter as a function of time, (b) PCFs after 0.3 s, and (c) interparticle spacing after 0.3 s. Increased particle speeds produced by ion drag at higher powers lead to lower values of  $\Gamma$ . Coulomb solids form at low to medium powers, and liquids form at high powers. A phase transition occurs between 16 and 20 W. Increasing electron densities at higher rf powers reduce the shielding length of particles, thereby allowing smaller interparticle distances.

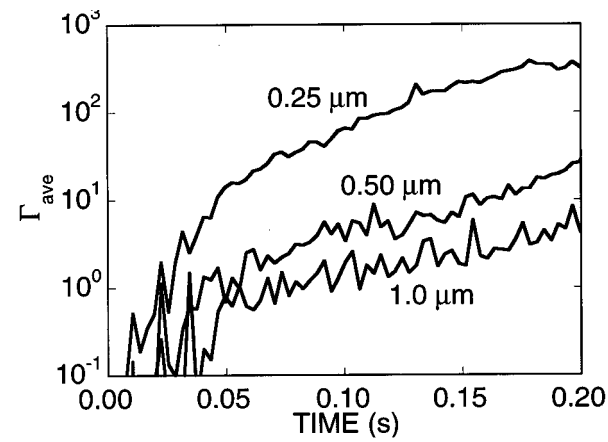
form at higher powers, when they do form, the interparticle spacing is smaller. The smaller spacing at high power results from two effects. The first is that at higher discharge powers the electron density is larger, thereby producing a smaller shielding distance which enables smaller  $d$ . The confining force, in this case largely a result of ion drag, is also larger at higher powers. Increasing power from 3.5 to 14.3 W results in a decrease in  $d$  from 212 to 182  $\mu\text{m}$ . This trend agrees with experimental findings.<sup>8-10</sup> Trottenberg *et al.*,<sup>9</sup> for example, found that increasing the power by a factor of 5 resulted in a decrease of  $d$  by a factor of 2.7, albeit for larger particles than studied here. This trend was also observed by Melzer *et al.*<sup>23</sup> They also found that the solid-liquid transition can be induced by lowering gas pressure, a consequence of the lower rate of particle cooling by fluid drag.

Although operating conditions largely determine the propensity to form Coulomb liquids and solids, particle size also influences both the rate of formation of these lattices and their ultimate structure. For example,  $\Gamma$  as a function of time, and PCFs after 0.2 s are shown in Fig. 6 for particles of varying radii. The discharge power is 7.3 W. The PCF for 1.0  $\mu\text{m}$  particles lacks significant structure. The corresponding  $\Gamma$  does not exceed 10, signifying that at best, a Coulomb liquid is formed. The PCF for 0.75 and 0.5  $\mu\text{m}$  particles shows distinct peaks, with corresponding values of  $\Gamma$  of 10s-100s. These particles form Coulomb solids. For these conditions, a phase transition between a Coulomb solid and liquid occurs at particle radii of 0.8-0.9  $\mu\text{m}$ . In order to generate Coulomb solids with larger particles, the discharge power must be lower or gas pressure higher; conditions which will produce more rapid cooling of the particles.

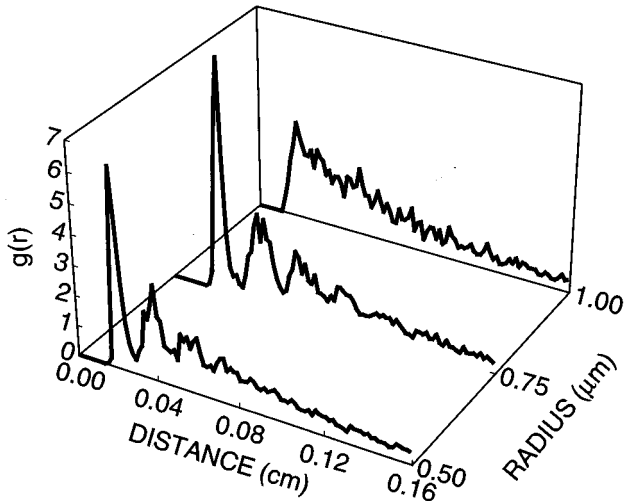
The interparticle spacing is also a function of particle size, as shown in Fig. 6(c). These spacings were derived from the PCFs. For small- to mid-sized particles ( $< \sim 0.8 \mu\text{m}$ ), interparticle spacing increases with increasing size. Since the Coulomb force scales as  $Q^2/r$ , and  $Q$  scales approximately as  $a$ , the force will scale as  $a^2/r$ . Therefore, increasing particle size will lead to larger Coulomb forces, and thus larger values of  $d$ . The ion drag force, however, increases with increasing particle size. This results in a higher particle temperature, which requires longer times for the lattice to form. However, when the lattice does form, the confining force provided by the ion drag is larger, thereby producing smaller interparticle spacing.

The cases discussed so far have been at constant gas pressure. With the exception of the "diffusion cooling" phenomenon, fluid drag is the cooling mechanism which is ultimately responsible for condensation of the crystal. It has been our observation, consistent with experimental results, that the phase transition between Coulomb solids and liquids shifts to higher discharge powers or larger particle size as the gas pressure increases. Analogously, the time required for the Coulomb solid to condense decreases with increasing gas pressure.

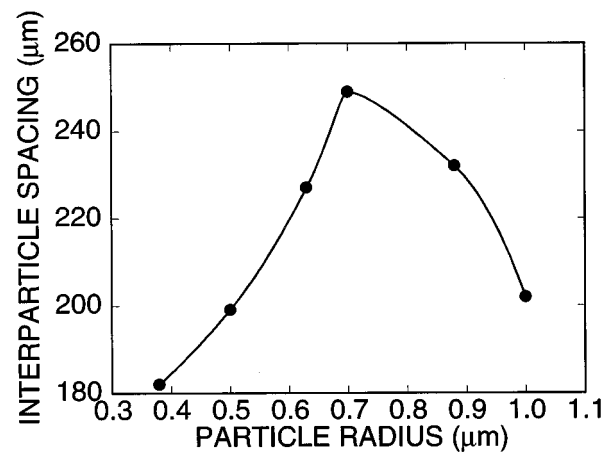
Experimental observations have shown that it is possible to "overload" a trap holding a dust particle cloud.<sup>7</sup> The observation is that once the trap is filled, adding a particle to the trap results in the ejection of another particle. We investigated this phenomenon using the geometry in Fig. 2. When



(a)



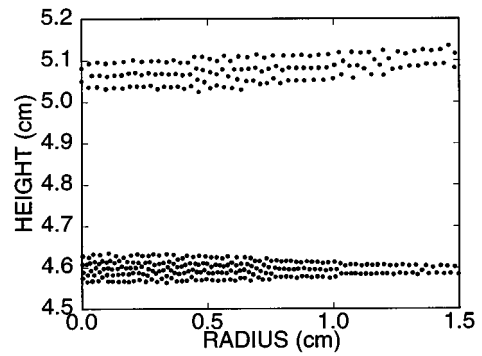
(b)



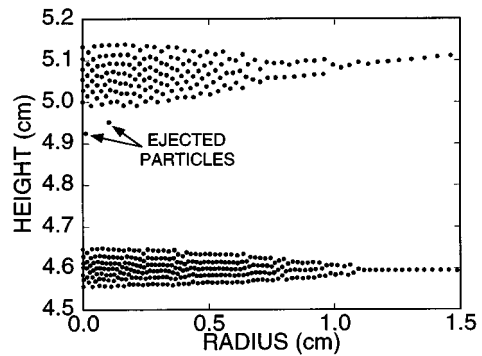
(c)

FIG. 6. Particle parameters while varying particle size. (a) Coulomb coupling parameter as a function of time, (b) PCFs after 0.3 s, and (c) interparticle spacing after 0.3 s. Smaller particles ( $<0.8 \mu\text{m}$ ) form lattices with interparticle distances that increase with increasing size, due to increased particle charges. Large particles are unable to readily form lattices due to their high temperatures. A phase transition occurs between 0.8 and 0.9  $\mu\text{m}$ .

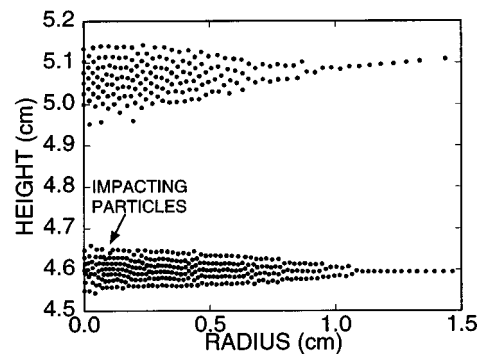
using 0.25  $\mu\text{m}$  particles, traps are formed near the powered (lower) and grounded (upper) sheath edges as shown in Fig. 7. Coulomb solids of 3–5 layers with well-defined PCFs and large  $\Gamma$  are formed. The lattice at the lower sheath edge has



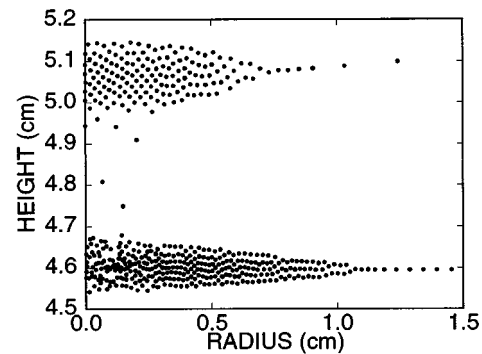
(a)



(b)



(c)



(d)

FIG. 7. Time progression of locations of 0.25  $\mu\text{m}$  particles illustrating overloading of traps and ejection of particles. Frame times are at (a) 0.104 s, (b) 0.191 s, (c) 0.200 s, and (d) 0.239 s. Particles condense and form two clouds due to the balance of ion drag and electrostatic forces. The upper trapping site fills and ejects particles as it continues to compress thereby increasing its particle density. Ejected particles strike the lower lattice creating dislocations. Continuous bombardment of particles effectively melts regions of the lower lattice.

a smaller interparticle spacing due to both the higher plasma density (shorter shielding distance) and larger confining forces. As time progresses, and more particles are added to the upper lattice, the width of the upper lattice increases, while the lattice contracts towards the center line due to electrostatic forces. When particles are added to the upper trap, their kinetic energy is dissipated into the lattice by collisions and they are cooled by fluid drag.

When the cumulative potential energy of the lattice exceeds the potential depth of the trap, adding an additional particle results in ejection of a particle. The ejected particles have significant potential energy, are first accelerated down towards the peak in the plasma potential by electrostatic forces. Once they pass the peak in the plasma potential, further acceleration occurs from ion drag. The ejected particles finally impact the lower lattice, at which time their kinetic energy is dissipated as heat in the lattice. This heat source lowers  $\Gamma$ , and disorders or melts the lower lattice. Particles continue to be ejected from the upper trap and the lower lattice continues to become increasingly disordered. The lattice disturbances propagate in both the  $r$  and  $z$  directions, but will eventually damp out due to fluid drag effects at which time the lattice refreezes.

This melting-freezing phase transition is further demonstrated in the sequence shown in Fig. 8. Here, we have generated a Coulomb solid in a positive column “pill box” cylindrical discharge sustained in 100 mTorr Ar with a peak ion density of  $10^9 \text{ cm}^{-3}$ , electron temperature of 3 eV, and without gas flow. A Coulomb solid of  $0.25 \mu\text{m}$  radius particles is formed near the axis having an interparticle spacing of approximately  $300 \mu\text{m}$ . A particle having  $\approx 1 \text{ keV}$  kinetic energy is directed into the Coulomb solid. The incident particle perturbs, and locally melts the lattice near its site of impact. The kinetic energy quickly dissipates in the lattice, is damped by fluid drag, and the crystal refreezes.

Another experimental observation is that Coulomb solids and well-ordered lattices are only obtained with fairly monodisperse particles. Lattices produced with particles having a distribution of sizes are less ordered. To investigate the degree of disordering which occurs with “impurities,” we generated a Coulomb solid of  $0.25 \mu\text{m}$  particles interspersed with 10% of  $0.2 \mu\text{m}$  particles. The resulting lattice and its PCF (with and without impurities) are shown in Fig. 9. The  $0.2 \mu\text{m}$  particle locations are shown by crosses and the  $0.25 \mu\text{m}$  particle locations are shown by closed circles. The PCF for the pristine lattice has at least six distinguishable peaks. The PCF for the contaminated lattice has less well-defined peaks and reduced long range order becoming amorphous. The smaller  $0.2 \mu\text{m}$  impurity particles hold less charge than the more numerous  $0.25 \mu\text{m}$  particles. As a result, a shorter interparticle spacing can be supported around the smaller particles. As the larger particles rearrange themselves to accommodate the smaller spacing, lattice dislocations are produced. We found that alloys of interspersed  $0.2$  and  $0.25 \mu\text{m}$  particles of nearly equal density (or a lattice  $0.25$  and  $0.3 \mu\text{m}$  particles) may, in fact, have a large  $\Gamma$  and for that reason can be considered a Coulomb fluid or solid. However, the resulting PCFs lack long range structure, which indicates that the solid is essentially amorphous.

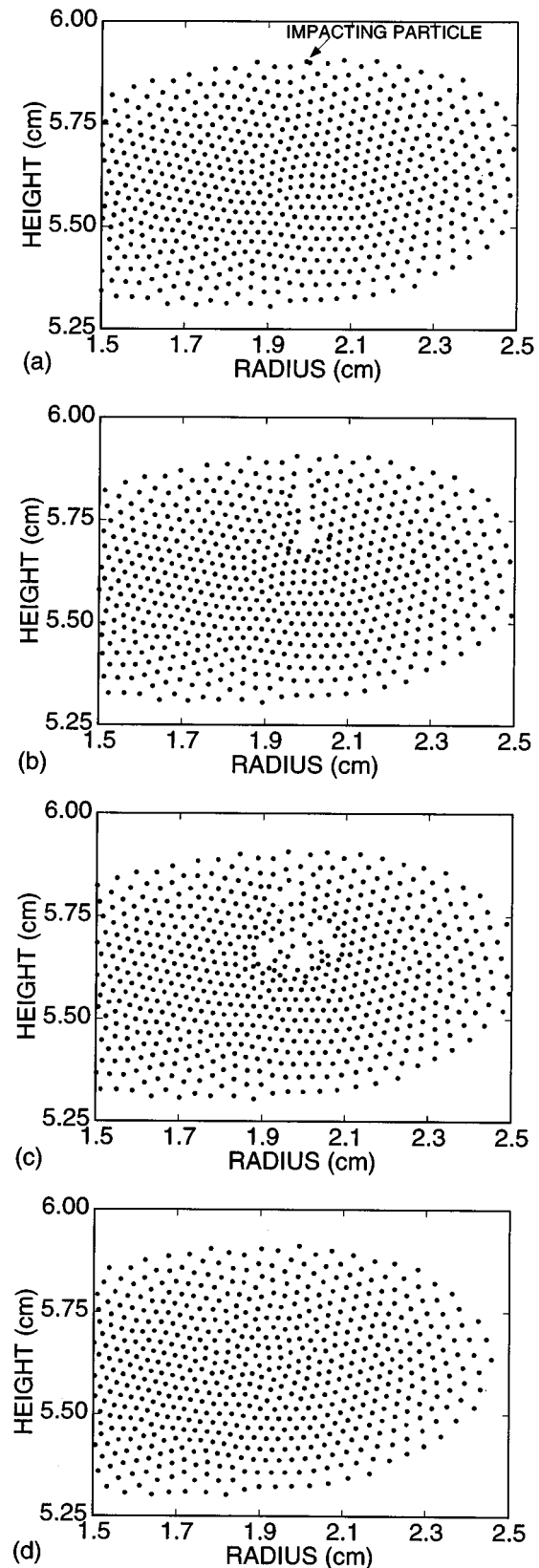
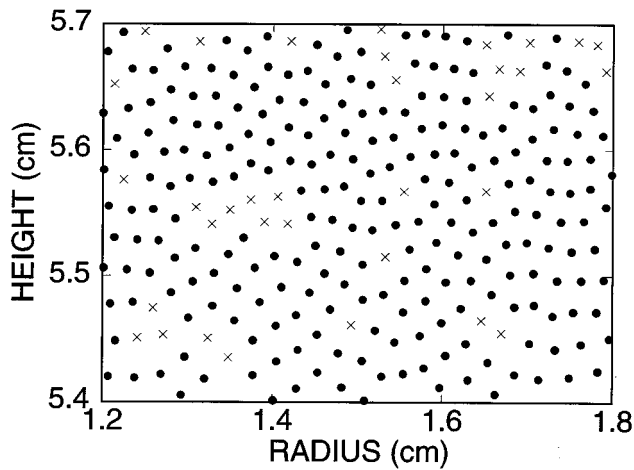
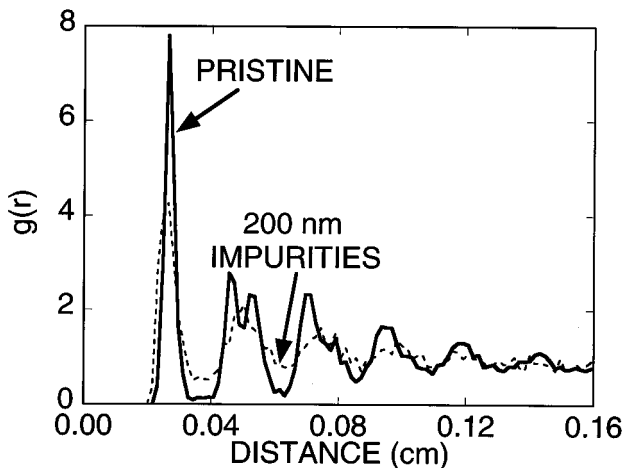


FIG. 8. Time progression of locations of  $0.25 \mu\text{m}$  particles illustrating local melting and refreezing of the lattice following injection of  $10 \text{ eV}$  particles. Frame times are at (a)  $0 \text{ s}$ , (b)  $2.4 \text{ ms}$ , (c)  $4.8 \text{ ms}$ , and (d)  $16 \text{ ms}$  after impact. The  $10 \text{ eV}$  injected particle creates a wavelike disturbance, which propagates and dissipates throughout lattice increasing the local temperature. Particles eventually refreeze, restoring the crystal shape after the disturbance damps out due to fluid-drag forces.



(a)



(b)

FIG. 9. Consequences of 10%  $0.2 \mu\text{m}$  particle impurities in a Coulomb solid made of  $0.25 \mu\text{m}$  particles. (a) Particle locations and (b) PCF with and without impurities. The presence of the impurities produces a small decrease in average interparticle size, and produces a decrease in long range order.

#### IV. CONCLUDING REMARKS

The formation of Coulomb fluids and solids by dust particles in RIE discharges was computationally investigated. We found that operating at low discharge power, high gas pressure, and with small particles produced conditions in which Coulomb solids will preferentially form. Increasing discharge power generates more energetic (higher temperature) particles and a lower  $\Gamma$ . Coulomb solids may, however, eventually form if dissipative fluid drag forces are suffi-

ciently high (high gas pressure) to cool the particles in traps, and increase  $\Gamma$ . The character of the resulting Coulomb solids, as indicated by  $g(r)$ , the pair correlation function, may be either crystalline or amorphous. Monodisperse particles generally form crystalline solids, while polydisperse particles form amorphous solids. Phase transitions between Coulomb liquids and solids were observed, as indicated by  $g(r)$ , when increasing particle size and rf discharge power.

#### ACKNOWLEDGMENTS

This work was supported by the Semiconductor Research Corporation, Sandia National Laboratories/Sematech, the National Science Foundation (CTS94-04133, ECS94-12565), and the University of Wisconsin Engineering Research Center for Plasma Aided Manufacturing.

- <sup>1</sup> Collections of papers addressing particle transport in plasma processing reactors appears in the following Special Issues: *Plasma Sources Sci. Technol.* **3**, No. 3 (1994); *J. Vac. Sci. Technol. A* **14** (1996).
- <sup>2</sup> G. S. Selwyn, J. E. Heidenreich, and K. L. Haller, *Appl. Phys. Lett.* **57**, 1876 (1990).
- <sup>3</sup> S. Ichimaru, *Rev. Mod. Phys.* **54**, 1017 (1982).
- <sup>4</sup> W. L. Slattery, G. D. Doolen, and H. E. DeWitt, *Phys. Rev. A* **21**, 2087 (1980).
- <sup>5</sup> H. Ikezi, *Phys. Fluids* **29**, 1764 (1986).
- <sup>6</sup> L. Boufendi, A. Bouchoule, R. K. Porteous, J. Ph. Blondeau, A. Plain, and C. Laure, *J. Appl. Phys.* **73**, 2160 (1993).
- <sup>7</sup> J. H. Chu, J.-B. Du, and I. Lin, *J. Phys. D* **27**, 296 (1994).
- <sup>8</sup> H. Thomas, G. E. Morfill, V. Demmel, J. Goree, B. Feuerbacher, and D. Möhlmann, *Phys. Rev. Lett.* **73**, 652 (1994).
- <sup>9</sup> Th. Trottenberg, A. Melzer, and A. Piel, *Plasma Sources Sci. Technol.* **4**, 450 (1995).
- <sup>10</sup> J. B. Pieper, J. Goree, and R. A. Quinn, *J. Vac. Sci. Technol. A* **14**, 519 (1996).
- <sup>11</sup> R. T. Farouki and S. Hamaguchi, *Appl. Phys. Lett.* **61**, 2973 (1992).
- <sup>12</sup> S. J. Choi, P. L. G. Ventzek, R. J. Hoekstra, and M. J. Kushner, *Plasma Sources Sci. Technol.* **3**, 418 (1994).
- <sup>13</sup> H. H. Hwang and M. J. Kushner, *Appl. Phys. Lett.* **68**, 3716 (1996).
- <sup>14</sup> F. Melandso and J. Goree, *J. Vac. Sci. Technol. A* **14**, 511 (1996).
- <sup>15</sup> J. E. Daugherty, R. K. Porteous, M. D. Kilgore, and D. B. Graves, *J. Appl. Phys.* **72**, 3934 (1992).
- <sup>16</sup> M. D. Kilgore, J. E. Daugherty, R. K. Porteous, and D. B. Graves, *J. Appl. Phys.* **73**, 7195 (1993).
- <sup>17</sup> S. J. Choi and M. J. Kushner, *Trans. Plasma Science* **22**, 138 (1994).
- <sup>18</sup> P. L. G. Ventzek, M. Grapperhaus, and M. J. Kushner, *J. Vac. Sci. Technol. B* **12**, 3118 (1994).
- <sup>19</sup> W. Z. Collison and M. J. Kushner, *Appl. Phys. Lett.* **68**, 903 (1996).
- <sup>20</sup> M. J. Kushner, W. Z. Collison, M. J. Grapperhaus, J. P. Holland, and M. S. Barnes, *J. Appl. Phys.* **80**, 1337 (1996).
- <sup>21</sup> H. W. Ellis, R. Y. Pai, E. W. McDaniel, E. A. Mason, and L. A. Viehland, *At. Data Nucl. Data Tables* **17**, 177 (1976).
- <sup>22</sup> R. A. Quinn, C. Cui, J. Goree, J. B. Pieper, H. Thomas, and G. E. Morfill, *Phys. Rev. E* **53**, R2049 (1996).
- <sup>23</sup> A. Melzer, A. Homann, and A. Piel, *Phys. Rev. E* **53**, 2757 (1996).